

Article

Design and Optimization of a Large Turboprop Aircraft

Fabrizio Nicolosi , Salvatore Corcione *, Vittorio Trifari  and Agostino De Marco 

Department of Industrial Engineering, University of Naples Federico II, Via Claudio 21, 80125 Naples, Italy; fabrnico@unina.it (F.N.); vittorio.trifari@unina.it (V.T.); agostino.demarco@unina.it (A.D.M.)

* Correspondence: salvatore.corcione@unina.it

Abstract: This paper proposes a feasibility study concerning a large turboprop aircraft to be used as a lower environmental impact solution to current regional jets operated on short/medium hauls. An overview of this market scenario highlights that this segment is evenly shared between regional turboprop and jet aircraft. Although regional jets ensure a large operative flexibility, they are usually not optimized for short missions with a negative effect on block fuel and environmental impact. Conversely, turboprops represent a greener solution but with reduced passenger capacity and speed. Those aspects highlight a slot for a new turboprop platform coupling higher seat capacity, cruise speed and design range with a reduced fuel consumption. This platform should operate on those ranges where neither jet aircraft nor existing turboprops are optimized. This work compares three different solutions: a high-wing layout with under-wing engines installation and both two- and three-lifting-surface configurations with low-wing and tail tips-mounted engines. For each concept, a multi-disciplinary optimization was performed targeting the minimum block fuel on a 1600 NM mission. Optimum solutions were compared with both a regional jet such as the Airbus A220-300 operated on 1600 NM and with a jet aircraft specifically designed for this range.

Keywords: aerospace; aviation; aeronautics; aircraft; design; open access; special issue; MDPI; turboprop; regional market; MDAO; innovative; green aviation



Citation: Nicolosi, F.; Corcione, S.; Trifari, V.; De Marco, A. Design and Optimization of a Large Turboprop Aircraft. *Aerospace* **2021**, *8*, 132. <https://doi.org/10.3390/aerospace8050132>

Academic Editor: Dieter Scholz

Received: 26 February 2021
Accepted: 25 April 2021
Published: 6 May 2021

Publisher's Note: MDPI stays neutral with regard to jurisdictional claims in published maps and institutional affiliations.



Copyright: © 2021 by the authors. Licensee MDPI, Basel, Switzerland. This article is an open access article distributed under the terms and conditions of the Creative Commons Attribution (CC BY) license (<https://creativecommons.org/licenses/by/4.0/>).

1. Introduction

From a preliminary overview, nowadays, the regional aircraft market segment is mainly influenced by a combination of three factors. A first key parameter to be considered is the environmental impact reduction, as can be seen by ever-more ambitious targets envisaged by international associations such as the Air Transport Action Group (ATAG) and the International Air Transport Association (IATA) or the Clean Sky 2 consortium. In 2008, the ATAG board developed a set of environmental goals for the short, medium, and long term which were supported and reiterated by the IATA Board and the association's Annual General Meeting [1]. Those goals can be summarized in the followings: an average improvement in fuel efficiency of 1.5% per year from 2009 to 2020; a cap on net aviation CO₂ emissions from 2020 (carbon-neutral growth); and a reduction in net aviation CO₂ emissions of 50% by 2050, relative to 2005 levels. However, as pointed out in [2], most of the targets forecasted by IATA and ATAG for 2020 have not been achieved, and the expected carbon-neutral growth appears to be quite far. This highlights the need to stress even more the reduction of the civil aviation environmental impact as the main driving parameter in the design of new and greener aircraft models.

In terms of innovation aiming at reducing civil aviation environmental impact, the Clean Sky 2 Program of Horizon 2020 has accelerated by now the development and introduction of new technologies designed for entry into service in the 2025–2035 timeframe. According to the Clean Sky 2 development plan, by 2050, 75% of the world's fleet now in service (or on order) will be replaced by aircraft that can deploy Clean Sky 2 technologies [3]. High level objectives defined by Clean Sky 2 expects a reduction in CO₂, NO_x, and environmental noise from –20% to –30% in the 2014–2024 timeframe. Furthermore,

reductions of -75% in CO_2 , -90% in NO_x , and -60% in environmental noise have been forecast by 2050.

In addition to the environmental impact topic, a second main factor currently influencing almost all market segments is represented by the recent COVID-19 outbreak, which has caused severe damage to the worldwide aviation industry.

Market forecasts made by the most important aircraft manufacturers at the beginning of 2020 have been completely changed by this unexpected event resulting in an overall reduction of air passengers (both international and domestic) of 50% in 2020 compared to 2019 [4]. In addition, the latest estimates made by the International Civil Aviation Organization (ICAO) [4] have highlighted a passenger demand drop from the 2020 originally planned forecasts by 2690 million (-60%), which has been related to a 370 billion US\$ loss of gross passenger operating revenues. A partial recovery has been forecast by ICAO [4] for the first half of 2021 reducing the passenger revenue loss faced in 2020, equal to $-369,768$ million US\$, to a value between $-178,373$ and $-148,719$ million US\$.

However, when a full recovery from COVID-19 damages will be reached, most major airlines will still have to face the third main factor influencing the regional market scenario, which is represented by the need to replace several hundred heritage aircraft, especially in the segment from 20 to 150 seats, which are now close to the end of their useful commercial life.

The combination of all these factors will deeply influence the current aviation industry shaping the new generation of aircraft. On the one side, ever more mutable and demanding requirements will be asked by the market, resulting in a very challenging design process to come up with new aircraft solutions. On the other side, in the near future, new ways and possibilities will be accessible to the aerospace research sector with innovative technologies and disruptive new aircraft concepts probably making their appearance on the upcoming market scenario.

To have an idea of which could be possible future market needs in the post-pandemic scenario, especially in the regional market segment, some interesting information can be obtained from recent market analyses made by the major aircraft manufacturers concerning the small single-aisle aircraft segment up to 150 seats.

Dealing with possible future aircraft requirements, Airbus Global Market Forecast (Airbus S.A.S., Blagnac, France) [5] provides a useful statistical trend which highlights a continuous increment in average seats capacity and mission ranges for the single-aisle jet fleet. Figure 1 shows that up to 2017 aircraft seats average has increased from 140 to 169, while average mission ranges have experienced an increment from 422 NM to 586 NM. Figure 1 also highlights that there is a significant variation around the mean which can be attributed to different aircraft sizes. In addition to showing the wide spectrum of operations for which the airlines use these aircraft, Figure 1 demonstrates why the range capability of aircraft products is an important consideration for airlines and manufacturers, a capability which also equates to flexibility.

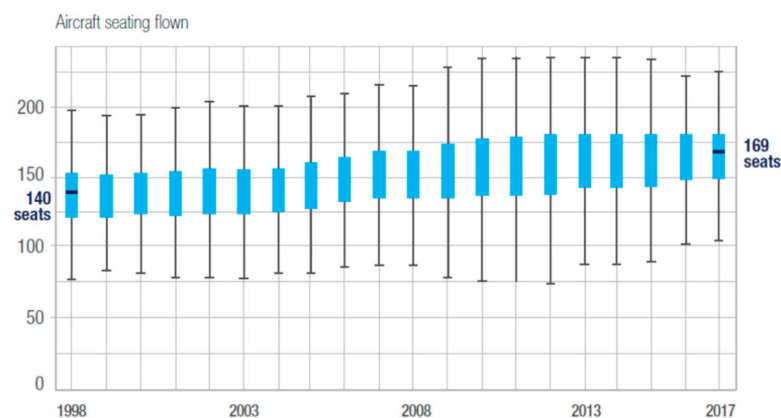


Figure 1. Cont.

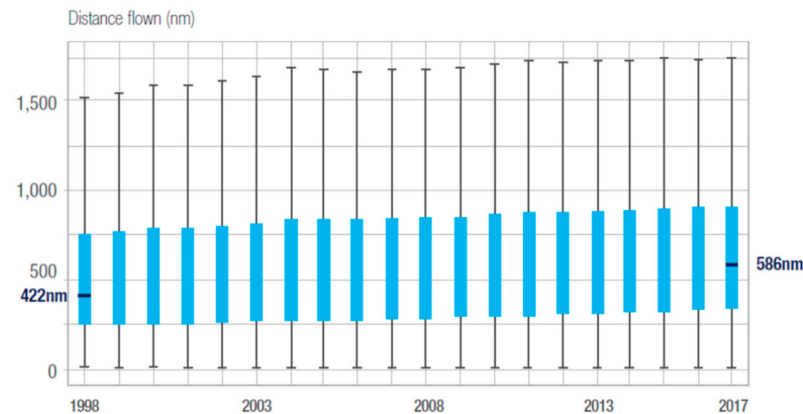


Figure 1. Distribution of single-aisle aircraft seats and ranges over the years. Reprinted from ref. [5].

As shown in Figure 2, up to 2016, both turboprop and regional jet aircraft were sharing the regional market evenly with a slightly increasing advantage of regional jets due to a higher seat capacity and longer mission distances than conventional regional turboprops. However, despite the regional jets success, turboprop engines are 10–30% more efficient than jet engines in terms of Specific Fuel Consumption (SFC), leading to a potential reduction of the amount of fuel used per mission as well as pollutant emissions. In fact, according to ATR forecasts [6], assuming all short haul flights operated by regional jets today are replaced by modern turboprops, 11% of overall regional aviation CO₂ emissions could be saved.

To design an advanced turboprop aircraft that could be competitive with respect to regional jets on short and medium haul, several key aspects must be assessed if compared to conventional turboprop designs. There is the need to increase the seats capacity, the aircraft must be designed for longer missions, and cabin noise and passenger comfort must be improved, as well as both the aerodynamic efficiency and the maximum cruise speed.

The authors have already faced the design of an advanced turboprop coupling higher seat capacity, improved cruise speed, and longer design range with a reduced fuel consumption within the framework of the European funded project named Innovative turbopROP configurationN (IRON) [7–12]. The project deals with the design of an innovative large turboprop aircraft with rear engine installation.

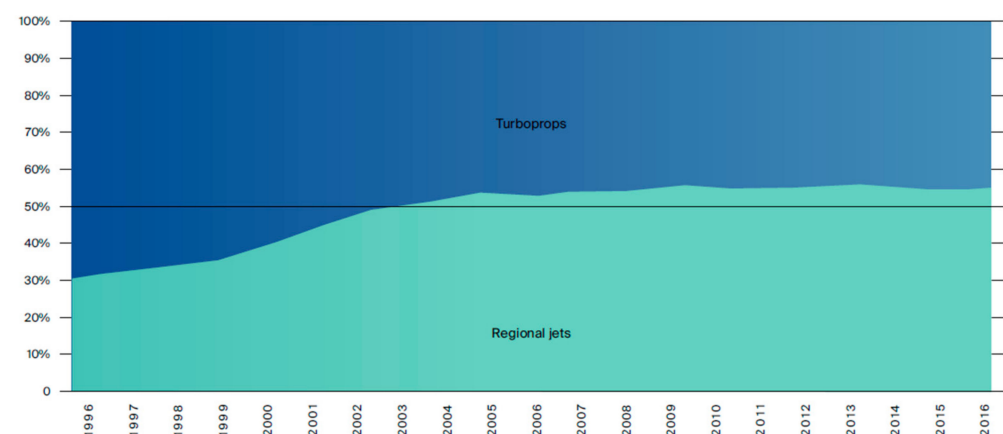


Figure 2. In-service fleet share of turboprops and regional jets. Reprinted from ref. [13].

Such a configuration shows several design issues dealing with the rear engine installation. The most comprehensive reference dealing with all key design aspects for a high-capacity propeller driven aircraft, including the rear engines installation, is the study performed by Goldsmith in [14], where a feasibility studies related to a possible conversion

of the McDonnell Douglas (Saint Louis, MO, USA) DC-9 from turbofan to turbo/prop-fan power plant is discussed.

Goldsmith's work shows useful evaluations dealing with the aircraft configuration feasibility, aerodynamics, weights, balance, and performance identifying three promising configurations with respect to the reference aircraft platform assumed as the DC-9 Super 80. The configurations proposed by Goldsmith exploited the results of the research programs carried out by NASA to develop technologies needed to implement potential fuel savings by adopting advanced turboprop engine architectures. These works highlighted 15–30% savings in aircraft block fuel compared to the state-of-the-art turbofan at the time by adopting advanced turboprop engines characterized by multi-bladed and high efficiently propellers that could be used at higher Mach numbers [15,16].

The selection of the most suitable configurations was made after a first qualitative comparison between many different possible layouts, followed by a multi-disciplinary quantitative analysis of three possible solutions. The first layout was an upper-wing-mounted propfan, indicated as Configuration 1 in Figure 3; the second one was a T-tail configuration with aft fuselage-mounted propfan, named Configuration 2 in Figure 3; and the last aircraft concept provided for a horizontal tail-mounted propfan, indicated as Configuration 3 in Figure 3. All modifications to the baseline platform were made by keeping constant both wing area and Maximum Take-Off Weight (MTOW) of the aircraft.

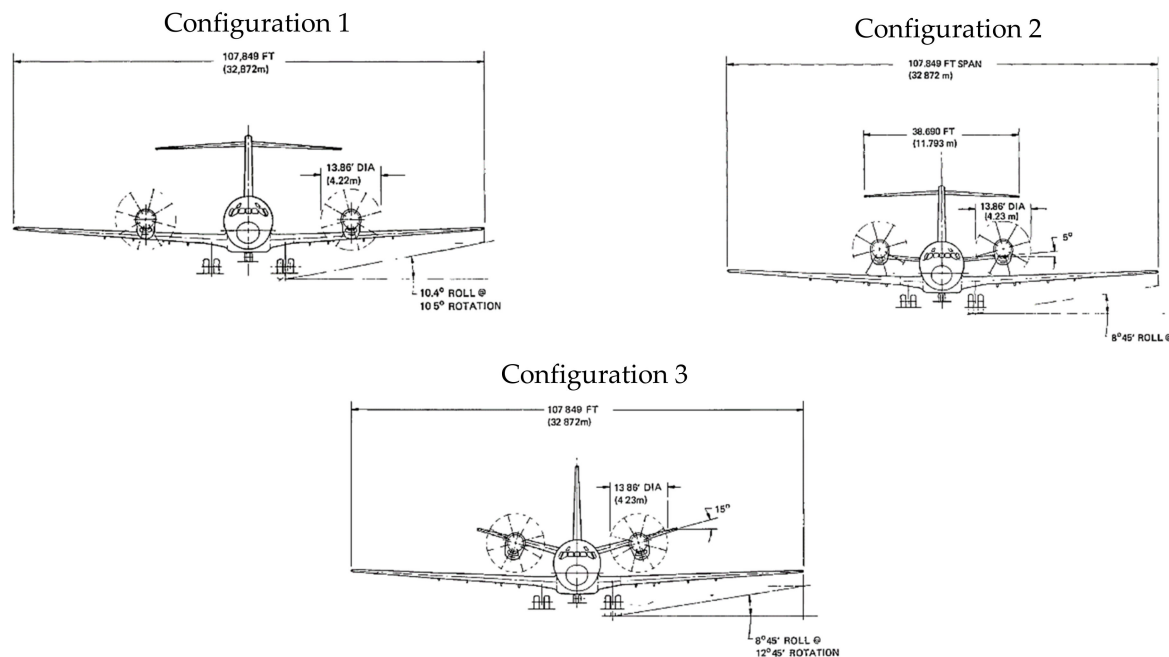


Figure 3. Configuration selected by the NASA feasibility study. Reprinted from ref. [14].

As shown in [14], the first and third layouts were identified as promising solutions providing for a block fuel reduction of about 14% and a mean Direct Operating Cost (DOC) reduction ranging from 6% to 8% with respect to the reference aircraft. The rear-mounted engines installation provided a much larger center of gravity excursion, a higher horizontal tail weight, and higher values of the equivalent parasite area. However, while the T-tail configuration led to lower performance and DOC improvements than the wing-mounted engines installation, the horizontal tail-mounted engines layout mitigated the above-mentioned negative effects, allowing to reach similar, or even better, performance and DOC improvements, if compared with the conventional wing-mounted engine configuration. Moreover, in the case of turboprop or open rotors, rear engine installation reduces the cabin noise providing for a better passenger's comfort.

The high propulsive efficiency of propellers nowadays still makes them quite an attractive solution for regional aircraft flying up to high subsonic speeds. Different concepts for a

large turboprop aircraft can be found in the literature. A novel concept for highly efficient and ecological propeller driven aircraft is proposed in [17]. This aircraft, characterized by a high wing, T-tail, and four turboprop engines with large propeller diameters, has shown a potential Direct Operating Cost (DOC) reduction of about 11% while reducing trip fuel mass and therefore CO₂ emissions by about 14.9% compared to the reference aircraft Airbus A320 (Airbus S.A.S., Blagnac, France). A modified architecture of the concept proposed in [17] is shown in [18]. This solution, featured by a strut-braced wing with natural laminar flow, could potentially reduce fuel consumption and CO₂ emissions by about 36% with respect to a reference jet aircraft (A320). In addition, DOC could be potentially reduced by about 17% on a mission range of 755 NM. The improvements mainly come from the lower fuel consumption of turboprop engines compared to turbofan engines. Drawbacks are the 21% increase in block time due to the lower cruise speed compared to a jet aircraft and the additional mass due to the higher landing gear lengths caused by high propeller diameters.

Recent studies concerning innovative turboprop aircraft designs are shown in [19], where two configurations featuring tail-mounted propeller and fuselage-mounted ducted propellers have been assessed in terms of their key performance indicators assuming they are designed for a harmonic mission of 1530 km and 68 passengers and compared with a conventional aircraft with wing-mounted propellers similar to ATR-72-600 in terms of geometry and weight.

Although previous research works have already dealt with the comparison between existing turbofan aircraft and future turboprop models to highlight possible improvements in environmental impact and DOC, none of them starts from the design of a modern turboprop aircraft based on a set of Top-Level Aircraft Requirements (TLARs) related to a short/medium haul (e.g., 1600 NM) coupled with a seat capacity in line with market analysis trends (e.g., 130–150 seats). Conversely, they start from an existing turbofan platform trying to make a conversion to a different propulsive system. In addition, most of the studies are focused on aircraft designed for longer missions with a slightly higher passenger number, or they focus the attention on smaller aircraft with similar design ranges but with a lower passenger capacity.

This work aims to investigate the combination of the selected mission range and seats capacity to design and optimize a possible modern turboprop platform suitable for an entry into service expected by 2035 and targeting the minimum environmental impact. Since there are no existing regional turbofans specifically designed for such a design range and seats capacity, this work does not limit its application in comparing the provided turboprop solutions with the current state of the art regional jet but also faces the design and optimization of a completely brand-new jet platform to perform fair comparison between a turboprop and jet driven aircraft both optimized for the same set of TLARs.

Such a comparison could represent useful information for aircraft designers who want to develop new aircraft suitable for regional applications by providing a good starting point in the decision process related to the preliminary design phase.

2. Aircraft Requirements and Critical Issues

The feasibility study starts from the definition of a specific set of TLARs, suitable for modern regional transport applications and in line with the main aircraft manufacturer market forecast, which is better illustrated in the Introduction. The TLARs driving the design of a large capacity turboprop are summarized in Table 1. As can be appreciated by looking at Table 1, to design a turboprop that could be competitive with respect to regional jets, there is the need to increase the seats capacity, as well as reduce the specific fuel consumption and the associated emissions. The cabin comfort must be improved by reducing the perceived noise and maximum aerodynamic cruise efficiency, the cruise speed value must be higher than the currently flying turboprop, and maximum lift coefficients at take-off and landing must be increased to be attractive with respect to regional jets in terms of ground performance.

Table 1. Topic Level Aircraft Requirements (TLARs).

Performance Requirements	
Passenger Capacity	130 pax at 32"
Range	1600 NM at Max payload (108 kg per pax), usual reserve (alternate + holding + reserves)
Cruise Speed	At FL300 ISA at 97% MTOW Mach (0.64–0.68)
Time to Climb	At MTOW-ISA-from 1500 ft to FL250 \leq 16 min
Take off Field Length (TOFL)	ISA-SL at MTOW, TOFL \leq 4600 ft (1400 m)
Landing Field Length (LFL)	ISA-SL at MLW, LFL \leq 4600 ft (1400 m)

Starting from the work shown by Goldsmith [14] and exploiting the lesson learned within the frame of the European project IRON [7–12], the authors made several considerations about different aircraft configurations that can be drafted in facing the design of a large turboprop aircraft.

The increase of the number of passengers from 70 to 130–150 leads to heavier aircraft, which means having a larger wing area and increased wingspan, affecting both the size and weight of the landing gears, as well as their positions to keep similar ground performance. According to the ICAO/Federal Aviation Administration (FAA) [20] span category, for aircraft in this class, the wingspan is limited to 36.0 m. Moreover, to ensure ground stability requirements due to a heavier aircraft with a larger wingspan, a larger wheel track is required as well.

A conventional high-wing configuration can accommodate large propellers and could be a possible solution for a high-capacity turboprop. However, for the high-wing configuration, two landing gear installations are suitable, as shown in Figure 4: nacelle-mounted or fuselage-mounted within fuselage pods. These two solutions may lead to several issues if used for high-capacity turboprops. The nacelle-mounted landing gears would require very long and heavy legs, which may be difficult to retract inside the nacelles, while fuselage-mounted landing gear might require quite large and heavy pods to ensure an adequate wheel track. Moreover, for both these layouts, the length of the landing gear legs must be increased to achieve a sufficient value of the upsweep angle due to a longer fuselage.

**Figure 4.** Landing gear installation solution for a large propeller driven aircraft.

A low-wing configuration could solve this issue. However, as shown by the example in Figure 5, a high-capacity turboprop will need a large propeller diameter to comply with an increased thrust requirement due to a higher weight (about 12–14 ft according to the estimations made within the EU CS2 IRON project). Thus, it would be impossible to ensure the required engine clearance from the ground.

For these reasons, a new turboprop aircraft configuration should be characterized by a rear-mounted engine installation. This can lead to a more efficient wing, thanks to the possibility to extend the laminar flow region and reduce the cabin noise by installing engines far from the cabin. Conversely, such an engine installation would lead to a wing weight increment (no mass relief on the wing loading due to the weight of the engines). Furthermore, this configuration can provide for a very large center of gravity (CG) excursion, which can also affect aircraft performance. A wide range of the CG excursion could imply a very large horizontal tail to trim the aircraft in the most rearward

CG positions, resulting in a reduction of maximum lift capabilities, while, at the most forward CG position, the longitudinal Static Stability Margin (S.S.M.) could be very high, requiring for a large download on the horizontal tail to trim the aircraft. This would reduce the aerodynamic cruise efficiency, affecting the fuel consumption and the aircraft DOC. One possible solution to mitigate this aspect consists in a reasonable cut of the overall CG excursion (by limiting the aircraft operability with low passenger number), complying with typical aircraft missions.



Figure 5. Large propeller installation issues for a low wing aircraft configuration.

Given all the above considerations, by looking at the feasibility study performed by NASA [14], and thanks to the experience matured within the IRON project, the authors identified in the rear-engine installation the most promising layout.

Following the work of NASA, the authors also investigated a conventional configuration with engines installed on the wing, with the difference that, in this research, the configuration with the upper wing engine installation was discarded because of both propeller and nacelle sizes. This layout was replaced by a conventional high-wing configuration with engines installed under the wing, assuming that the main landing gear could be installed in fuselage pods. Another difference with the feasibility study performed by NASA is that the T-tail configuration with the rear engine installation was replaced by a three-lifting-surface layout.

The T-tail layout could ensure an adequate longitudinal static stability, as well as cruise aerodynamic efficiency, while probably providing for poor high-lift capabilities and balance issues due to a very afterward mass concentration. Moreover, the installation of a large propeller (12–14 ft of diameter) would require a pylon with a non-negligible span, making the latter comparable to a tailplane.

This configuration was discarded from the first stage of design and replaced by a three-lifting-surface layout which could ensure the required longitudinal stability potentially increasing as well as both aerodynamic efficiency and high-lift capabilities.

The introduction of a third lifting surface could help reduce the tail download required to trim the aircraft. Thus, the trimmed maximum lift coefficient ($C_{L_{max}}$) could be increased while the trim drag contribution could be reduced, resulting in a higher value of the cruise aerodynamic efficiency. The potential increment of the $C_{L_{max}}$ could also lead to a reduced wing area providing for additional benefits on cruise aerodynamic efficiency as well as a reduction in aircraft weight (unless the third lifting surface would be heavier than the wing weight reduction).

Furthermore, the third lifting surface could allow to shift forward the aircraft neutral point position, as well as giving the possibility to optimize both the center of gravity excursion and the neutral point position, at fixed static stability margin, by changing wing, horizontal tail, and canard sizes together and their relative positioning. In short, the three lifting surfaces would extend the design space, allowing to cope with both aerodynamic cruise efficiency and maximum lift capabilities of the aircraft. In designing a three-lifting-surface aircraft, particular attention must be paid to evaluating the negative effects in terms of downwash introduced by the canard that acts on both the main wing and the horizontal tail, as shown in [9,11,12].

3. Investigation Workflow and Methods

Starting from the TLARs described in Table 1, for each of the considered aircraft configurations, a sensitivity analysis was carried out by changing the following design parameters:

- Wing planform (span, aspect ratio, sweep angle, and longitudinal wing position)
- Horizontal tail plane planform (span, aspect ratio, and sweep angle)
- Canard planform if present (span, aspect ratio, and longitudinal position)

The complete picture of the design space is shown in Table 2, where, for each of the previous design variables, the considered range of variation is indicated. A specific combination of the design parameters shown in Table 2 generates an aircraft that underwent to a Multi-Disciplinary Analysis process (MDA). The MDA involves all major disciplines of the preliminary aircraft design (i.e., weight, balance, aerodynamics, performance, and DOC). The single MDA cycle shown in Figure 6 and the full factorial Design of Experiments (DOE) represented in Table 2 were performed by means of JPAD (Java tool chain of Programs for Aircraft Design), software developed at the Industrial Engineering Department of the University of Naples Federico II [21–23].

JPAD includes several interconnectable analysis modules which can be used both in standalone mode and in a complete MDA cycle. One of the most important analysis modules is the one dedicated to the evaluation of the most important aircraft performance, which implements a smart simulation-based approach to analyze the complete mission profile including on-ground phases such as take-off and landing [24].

The analysis starts with a first estimation of the amount of fuel needed for the specified mission. Then, a balance analysis is carried out to determine the center of gravity excursion. For each center of gravity, the aerodynamic and stability module estimates the trimmed aircraft lift curve and the trimmed drag polar curve according to the following flight conditions: take off, climb, cruise, and landing. Finally, the performance module uses these data to make a detailed simulation of the initial mission profile estimating a new amount of fuel required to fulfill the mission. Thus, an iterative process is carried out until the first estimated fuel mass is equal to the one calculated by the mission profile analysis. Within the fuel mass iterative loop shown in Figure 6, a second nested iteration is carried out to make the take-off field length and cruise Mach number comply with the assigned TLARs. This is obtained by scaling the reference static thrust of all engines with a step of $\pm 2.5\%$. Together with this thrust scaling, engine weight is updated as well so that an intermediate weight convergence loop must be carried out as well. Both fuel mass and performance iterative loops have a maximum number of iterations fixed to 50. All configurations that do not converge within this limitation are supposed to be unfeasible so that a penalty will be added to those response surface points during the optimization process.

At the end of the convergence loop, other checks are performed on the analyzed configuration. These concern the operative maximum aft center of gravity position, which must be at least 5% of the wing Mean Aerodynamic Chord (MAC) more forward than the main landing gear position due to rotation issues, and the maximum fuel tank capacity, which must be greater than the estimated total mission fuel mass plus reserves.

The multidisciplinary optimization was carried out by imposing the following constraints:

- The minimum static stability margin (with the max aft. center of gravity position) must be greater than zero.
- Take-off and landing field lengths must be at most 1400 m.
- The time to climb from 1500 to 25,000 ft must be at most 16 min.
- The maximum cruise Mach number should be higher than 0.64 and should not exceed 0.68 to consider for propeller operative limitation in terms of compressibility issues.
- The distance between the main landing gear position (X_{LG}) and the maximum aft center of gravity position ($X_{CG,max,aft}$) must be greater than 5% of the mean aerodynamic chord to avoid ground stability issues.
- The estimated total mission fuel mass must be lower than wing fuel tank maximum capacity.

Table 2. Variables design space for each aircraft configuration.

Parameters	Wing Mounted Engines Configuration	Rear Mounted Engines Configuration	Three Lifting Surfaces
Wing Design Parameters			
Span b_w (m)	32.0–35.5	32.0–35.5	32.0–35.5
Longitudinal position $X_{LE,W}$ (m)	13.0–16.0	18.0–22.0	19.0–22.0
Aspect Ratio AR_w	9.8–13.3	10.2–13.8	10.2–13.6
Sweep at leading edge $\Lambda_{LE,W}$ (°)	2.5–10.0	2.5–10.0	2.5–10.0
Horizontal Tailplane Design Parameters			
Span b_H (m)	9.14–11.17	11.7–14.3	11.7–14.3
Longitudinal position $X_{LE,H}$ (m)	37.15 fixed value	30.0–32.0	30.0–32.0
Aspect Ratio AR_H	4.96 fixed value	4.40 fixed value	4.40 fixed value
Sweep at leading edge $\Lambda_{LE,H}$ (°)	$\Lambda_{LE,W} + 5.0$	$\Lambda_{LE,W} + 5.0$	$\Lambda_{LE,W} + 5.0$
Canard Design Parameters			
Span b_C (m)	n.a	n.a	7.2–8.8
Longitudinal position $X_{LE,C}$ (m)	n.a	n.a	5.0–8.0
Aspect Ratio AR_C	n.a	n.a	5.57 fixed value
Sweep at leading edge $\Lambda_{LE,C}$ (°)	n.a	n.a	10.0 fixed value
Total number of analyzed aircraft	972	6075	34,020

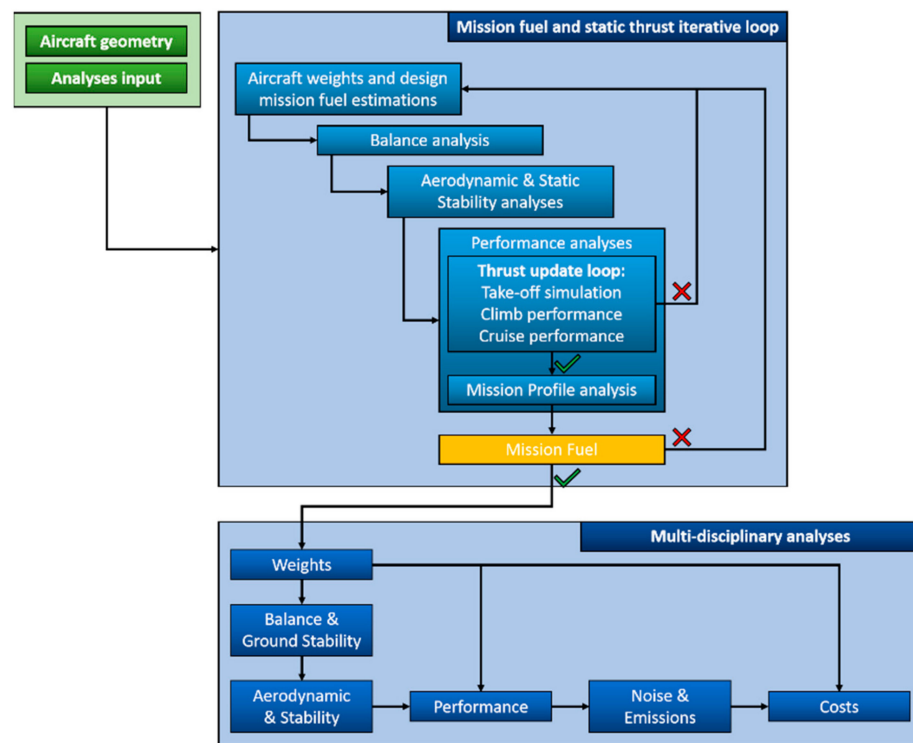


Figure 6. JPAD MDA workflow including thrust update inner loop.

All analyses were performed under several assumptions concerning masses and positions of main components, on-board systems, the center of gravity position to be used for each mission phase, fuel tank systems, laminar flow, and downwash effects (especially in the case of three-lifting-surface configuration). Fuselage length and maximum diameter were kept constant for all analyzed aircraft. Horizontal tailplane sweep angles at leading edge were assumed to be 5° greater than the related wing sweep angle at leading edge. Components and on-board systems masses were calculated using equations provided by Torenbeek [25], which indicate several corrections to be made according to the specific aircraft configuration. Center of gravity positions of the main aircraft

components were assumed according to Torenbeek [25] as well. Some assumptions were made concerning major on-board systems longitudinal position, as shown in Table 3. An example of aircraft components and on-board systems center of gravity position is shown in Figure 7 considering the case of a three-lifting-surface configuration.

Table 3. On-board systems assumptions for the MDA cycle of each aircraft configuration.

Assumption Concerning Systems and Equipment Positions	
Auxiliary Power Unit (APU)	87% fuselage length
Air Conditioning and Anti-Icing System	30% MAC ahead the wing root leading edge
Electrical System	42% fuselage length (half cabin)
Furnishings and Equipment	37% fuselage length
Control Surface Actuators	Using lifting surfaces positions weighted average with components masses
Instruments and Navigation System	8% fuselage length (cockpit)
Operating Items	21% fuselage length (close to the front galley)

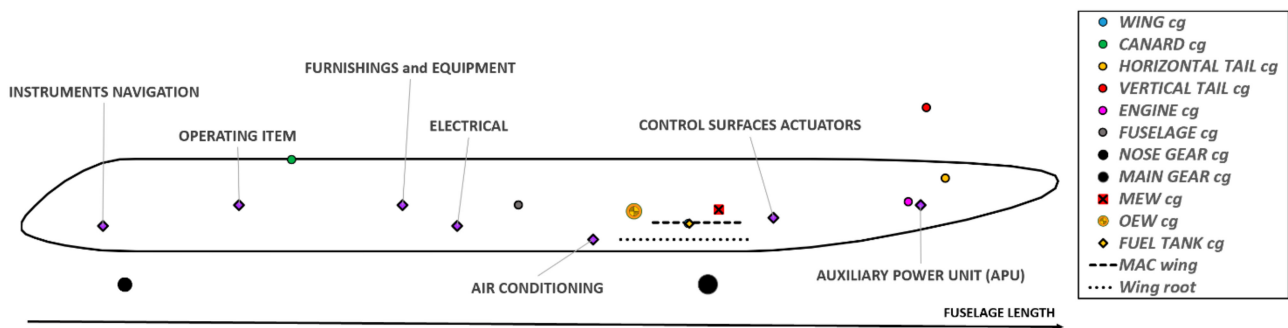


Figure 7. Example of aircraft main components and systems center of gravity positions for a three-lifting-surface configuration.

To take into account the aircraft weight reduction due to fuel consumption during the design mission, a variable center of gravity position must be considered for each phase, affecting in this way the aircraft stability and providing for a variable trim drag value. This effect was simulated by considering different center of gravity positions from the boarding diagram. For take-off and climb conditions, the maximum take-off weight center of gravity was considered. The cruise phase was evaluated assuming a center of gravity position related to an average fuel weight condition (starting from the maximum take-off weight). The landing condition was investigated assuming a center of gravity position related to the maximum landing weight (about 90% of the maximum take-off weight). Finally, the longitudinal static stability margin was estimated considering the most aft center of gravity position.

For each of the selected aircraft configurations, some assumptions and some technologies were envisaged, as shown in Figure 8 where their effects related to both aerodynamics (in terms of drag, maximum lift capabilities, and downwash on the horizontal tail plane) and weight estimation are summarized.





Technology	Wing-Mounted Engines			Rear-Mounted Engines			Three-Lifting Surfaces		
	Weight	Drag	Lift and Long. Stability	Weight	Drag	Lift and Long. Stability	Weight	Drag	Lift and Long. Stability
Wing NLF	-	-10dcs	-	-	-20dcs	-	-	-20dcs	-
 Fuselage LG and pods	+7%Fuselage	+15dcs (pods)	-	-	-	-	-	-	-
 Under-wing engine	-5%Wing	+ 10dcs	-0.2 C_{Lmax} Downwash at Htail 0.25 (at $M=0.2$)	-	-	-	-	-	-
 Rear-mounted engine at Htail tip	-	-	-	+5%Wing +4%Fuselage +65%Htail	-	+0.2 C_{Lmax} +10% C_{LaH} Downwash at Htail 0.32 (at $M=0.2$)	+5% Wing +4% Fuselage +65% Htail	-	+0.2 C_{Lmax} +10% C_{LaH} Wing-Tail downwash
 Canard Installation	-	-	-	-	-	-	+5% Fuselage	-	+0.15 C_{Lmax} Downwash at Htail 0.53 (at $M=0.2$)

Figure 8. Technological assumptions for each considered aircraft configuration.

Wing-mounted engines configuration. This is the state-of-the-art of conventional turboprop configuration with a high-wing and T-tail layout. Thus, the horizontal tail-plane position was fixed according to vertical tail tip chord position with a fixed incidence angle equal to 0.0° . Furthermore, the horizontal tailplane aspect ratio was fixed to about 5.0 with the possibility to scale the span and the planform area. Engines positions were linked to the starting section of the wing outer panel, assuming laminar flow effects to be active only on the outer wing panel. Landing gears were assumed to be mounted in fuselage pods. Their positions were linked to the wing position assuming that wing and landing gears attachments are applied to the same fuselage frame. Furthermore, landing gear pods provide for a higher parasite drag, which was modeled considering an increment of about 15 drag counts. According to Torenbeek [25], wing mass were reduced by 5% due to wing-mounted engines. To account for landing gear fuselage pod installation, a further reduction of 5% of the wing mass was considered. Spoilers' installation effect on wing weight was modeled assuming an increment of the component mass of 2% while, for the fuselage, Torenbeek [25] suggested increasing the estimated mass by 8% due to pressurization effects and by 7% due to landing gears pods.

Rear-mounted engines configuration. This innovative configuration provides for a low-wing configuration with engines installed at the horizontal tailplane tips. This solution would avoid a large engine pylon needed to install a large turboprop engine with a propeller diameter of about 12 ft on the fuselage.

A similar solution is also investigated in [26], where the main configuration criticalities dealing with aircraft weight and balance are highlighted.

From preliminary calculations made by the authors, this configuration will require for a large engine pylon affecting the aircraft aerodynamics and interfering with the horizontal tail plane. A solution could be the adoption of a T-tail configuration. However, a large

pylon would provide an additional lift contribution at high aircraft attitudes leading to a larger longitudinal static stability margin with a detrimental effect on maximum trimmed lift coefficients. Moreover, a T-tail configuration would provide for a heavier vertical tail plane (due to the horizontal tail installation), heavy pylons to hold engines, and a heavier fuselage due to additional structural frames required to hold all the rear aircraft components. Thus, the authors selected a simplified configuration merging the horizontal tail with the pylon. This solution, already investigated within the frame of the European funded project named IRON, could yield to a reduced overall mass increment as well as to provide for a reasonable value of the aircraft longitudinal stability. The horizontal tail is fuselage mounted, and it was assumed to have a variable pitch angle (i_H). The horizontal tailplane Aspect Ratio (AR_H) was fixed at 4.40 for structural considerations regarding the engine installation. Being the considered layout a low-wing configuration, landing gears were assumed to be wing-mounted. This will help to limit the required fuselage pods size to accommodate landing gear legs since only wheels and a small legs portion should be retracted inside them. Thus, the detrimental impact that large fuselage pods could have on fuselage weight and aerodynamic drag will be reduced. According to the selected main landing gear installation, its position was linked to the wing at 60% of the MAC. According to Torenbeek [25], wing mass was increased by 2% to consider for wing spoilers. Concerning the fuselage, Torenbeek [25] suggested increasing the estimated mass by 8% due to pressurization effects and by 4% due to rear engine installation. Moreover, the horizontal tailplane mass was increased by 65% on the base of preliminary evaluations of combined aerodynamic loading and engine inertial contributions. Unlike the wing, the horizontal tailplane usually works with negative aerodynamic loads, thus the engine mass does not provide for load relief effects. Thanks to the rear engine installation, the whole wing was supposed to work in laminar flow conditions, reducing the wing parasite drag of about 20 drag counts.

Three-lifting-surface configuration. This configuration, as well as the rear-mounted engine aircraft, provides for a rear engine installation at the horizontal tailplane tips. As for the previous layout, the horizontal tail was supposed to have a variable pitch angle according to the specific flight phase (same values assumed for the rear-mounted configuration) and the tail aspect ratio was kept constant at 4.40 due to structural reasons linked to the engine installation. The same horizontal tailplane mass increment of 65% was assumed due to the same structural considerations made for the rear-mounted engines solution. The same assumptions also applied for the main landing gear position, horizontal tail mass increment, and laminar flow effects on the wing. The amount of storable fuel is linked to the estimated tank capacity calculated assuming standard spar positions and using the volume equation proposed by Torenbeek [25].

4. Results

Once the MDA analysis cycle for each aircraft model investigated with the DOE was completed, results dealing with some of the most important design objectives were gathered. Figure 9a illustrates the complete cloud of points analyzed by the MDA process for the three-lifting-surface configuration in terms of block fuel versus maximum take-off weight and maximum aerodynamic cruise efficiency. In addition, Figure 9b,c show how the constraint on the static stability margin ($S.S.M. \geq 0.0$) reduces the number of possible candidate solutions in two different planes: block fuel versus maximum take-off weight and block fuel versus maximum aerodynamic cruise efficiency. Blue circles represent all solutions that are compliant with the imposed constraint on the S.S.M. The same applies for each additional constraint included in the optimization problem.

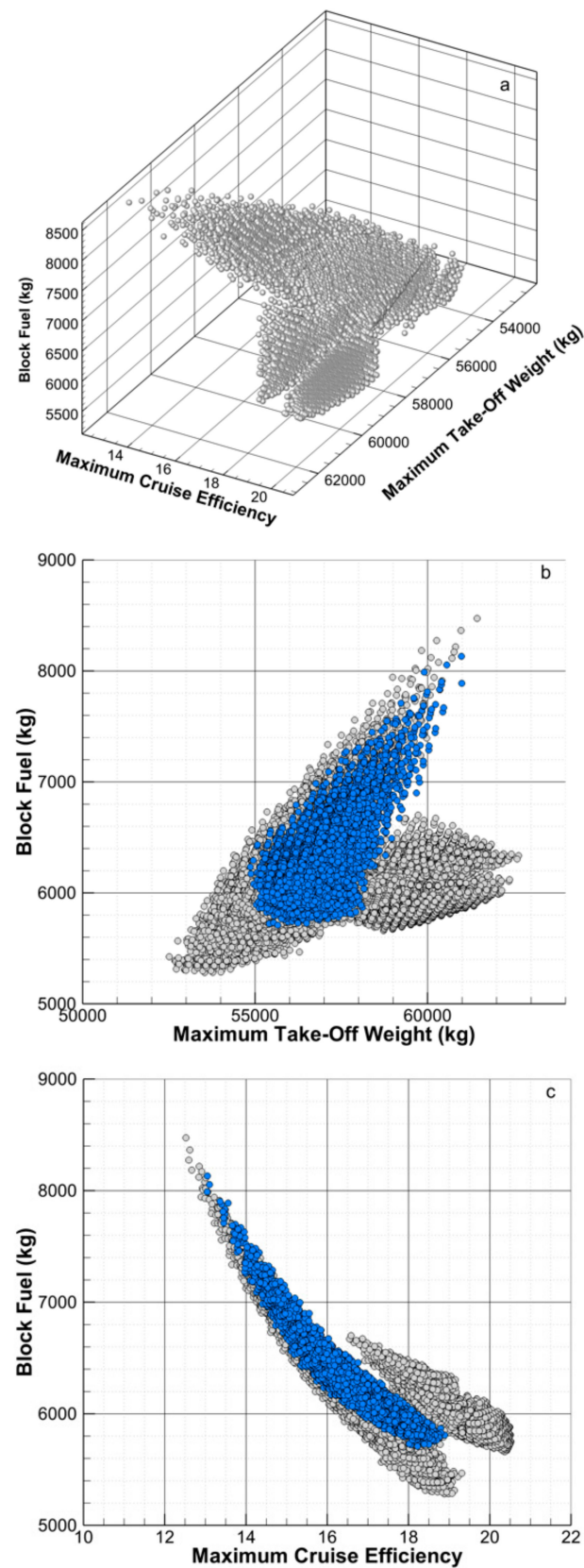


Figure 9. Results of design of experiments for the three-lifting-surface: (a) complete cloud of points; (b) effect of the S.S.M constraint on possible candidate solutions in the plane block fuel versus MTOW; and (c) effect of the S.S.M constraint on possible candidate solutions in the plane block fuel versus cruise maximum efficiency.

The optimization problem defined in Equation (1) was mainly focused on the minimization of the environmental impact provided by each configuration. Thus, the block fuel was considered as the only objective function.

$$\left\{ \begin{array}{l} \text{Minimize the Block fuel on a mission range of 1600 NM} \\ \text{with respect to lifting surfaces planform design variables and relative positioning} \\ \text{subject to :} \\ \text{S.S.M} \geq 0.0 \\ \text{Take - off field length \& Landing field length} \leq 1400 \text{ m} \\ \text{Climb time from 1500 ft to 25,000 ft} \leq 16 \text{ min} \\ \text{Cruise Mach number } 0.64 \leq M_{cr} \leq 0.68 \\ \left\| X_{LG} - X_{CG, \max, aft} \right\| \geq 5\% \text{MAC} \\ \text{Estimated mission fuel} \leq \text{Max storable fuel mass} \end{array} \right. \quad (1)$$

Although aircraft are typically designed aiming at minimizing the DOC, this quantity was not considered inside the objectives set. Main contributions to DOC are due to aircraft weight, cruise Mach number, and mission block fuel. However, concerning the aircraft weight for a fixed configuration, its variation inside the obtained response surface is mainly due to the mission block fuel. Thus, the effect of the aircraft maximum take-off weight on the DOC is strictly based on the block fuel variation. In addition, following the lessons learned from the EU project IRON, the response surface cruise Mach number variation was limited to a narrow range from 0.64 to 0.68. Those limits were driven by market requirements for the lower bound and by propeller tip compressibility issues for the upper bound. In this range, the effect of the cruise Mach number on the aircraft DOC resulted to be of second order with respect to the mission block fuel. For all these reasons and considering the additional limitations brought by the imposed set of constraints to the DOC value, the latter was not considered as an objective function. However, its value, in terms of both total and cash DOC, was monitored to make a comparison between the optimized configurations.

To demonstrate the above, Figures 10–12 show the variation of the estimated total DOC with respect to the block fuel for each analyzed configuration, highlighting all feasible solutions compliant with the imposed set of constraints. It must be noted that the minimum feasible block fuel almost corresponds to the minimum DOC solution. In addition, the range of variation of the total DOC value for each aircraft configuration resulted to be very limited.

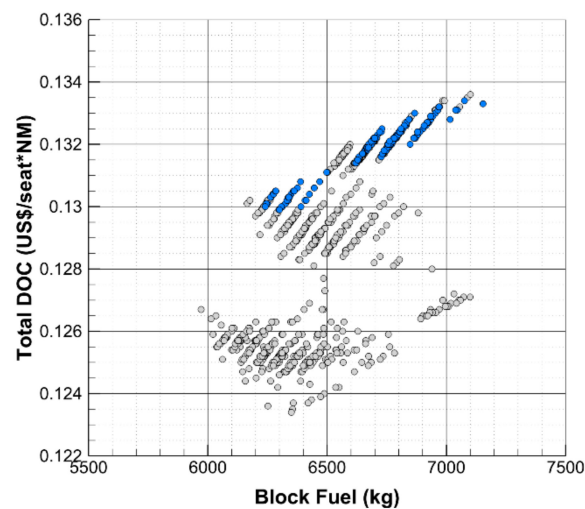


Figure 10. Total DOC versus block fuel for the wing-mounted engines configuration. Blue circles represent the solutions compliant with the imposed set of constraints.

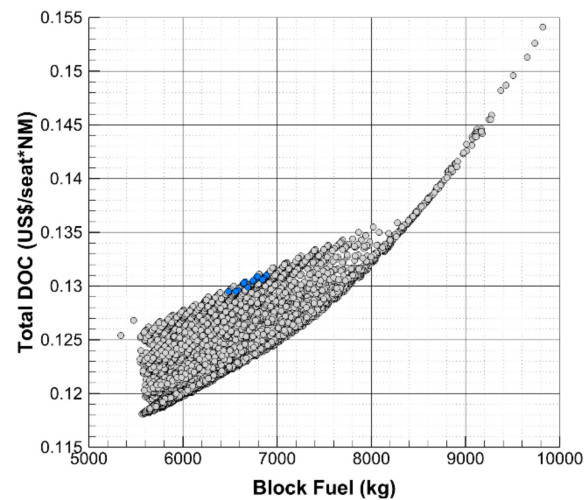


Figure 11. Total DOC versus block fuel for the rear-mounted engines configuration. Blue circles represent the solutions compliant with the imposed set of constraints.

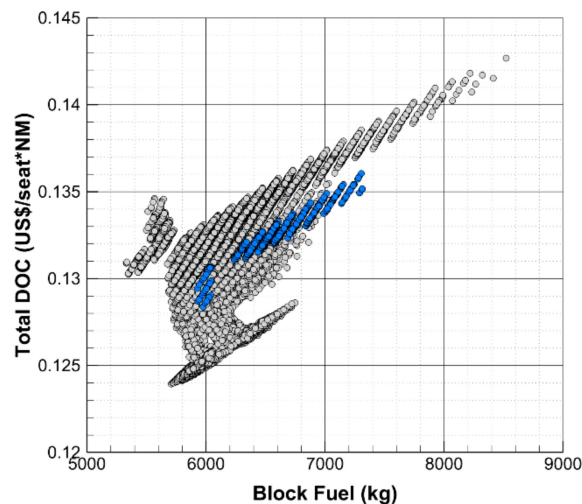


Figure 12. Total DOC versus block fuel for the three-lifting-surface rear-mounted engines configuration. Blue circles represent the solutions compliant with the imposed set of constraints.

Selected optima aircraft models are compared in Figure 13 including a visual representation of their center of gravity excursion, while their main characteristics are summarized in Table 4.

Both the wing- and rear-mounted engine aircraft are characterized by a wing area of about 105 m^2 and wing aspect ratio of about 12, while the three-lifting-surface aircraft has a reduced wing area (about 100 m^2) thanks to the additional lift contribution provided by the canard.

The two configurations with rear-mounted engines present a very large horizontal tail area (about 44% of the wing area) due to the need to balance a very large center of gravity excursion, as illustrated in the boarding diagrams from Figure 13.

Nevertheless, the three-lifting-surface configuration presents a higher aerodynamic cruise efficiency thanks to the positive effect of the forward lifting surface (the canard) on the global trim drag contribution. It is worth noticing that the total aircraft wetted area (which is linked to the parasite drag) is slightly higher for the three-lifting-surface compared with the rear-mounted engine configuration.

All three optimal configurations are stable with respect to the most aft center of gravity position with a reduced Static Stability Margin (S.S.M.), as shown in Table 4. In the authors'

opinion, the obtained S.S.M. value is acceptable and compliant with an improved flight control system, which is forecasted for entry into service 2035.

Using the main performance and DOC as rules of comparison of the three optimal large capacity turboprop configurations, the three-lifting-surface configuration was proven to be the best solution among the considered layouts. In fact, although with very similar values of ground performance, the three-lifting-surface aircraft provides for the lowest value of the block fuel, thanks to the improved cruise aerodynamic efficiency, as well as for the lowest maximum take-off weight.

Despite the additional component, the main reason behind the three-lifting-surface configuration reduced max take-off weight is related to the different engine weight coupled with a lower amount of block fuel. Focusing on the engine mass, this value was linked to the value of the static thrust inside the workflow in Figure 6, where, to match both the required take-off field length and cruise Mach number, the static thrust was adjusted iteratively.

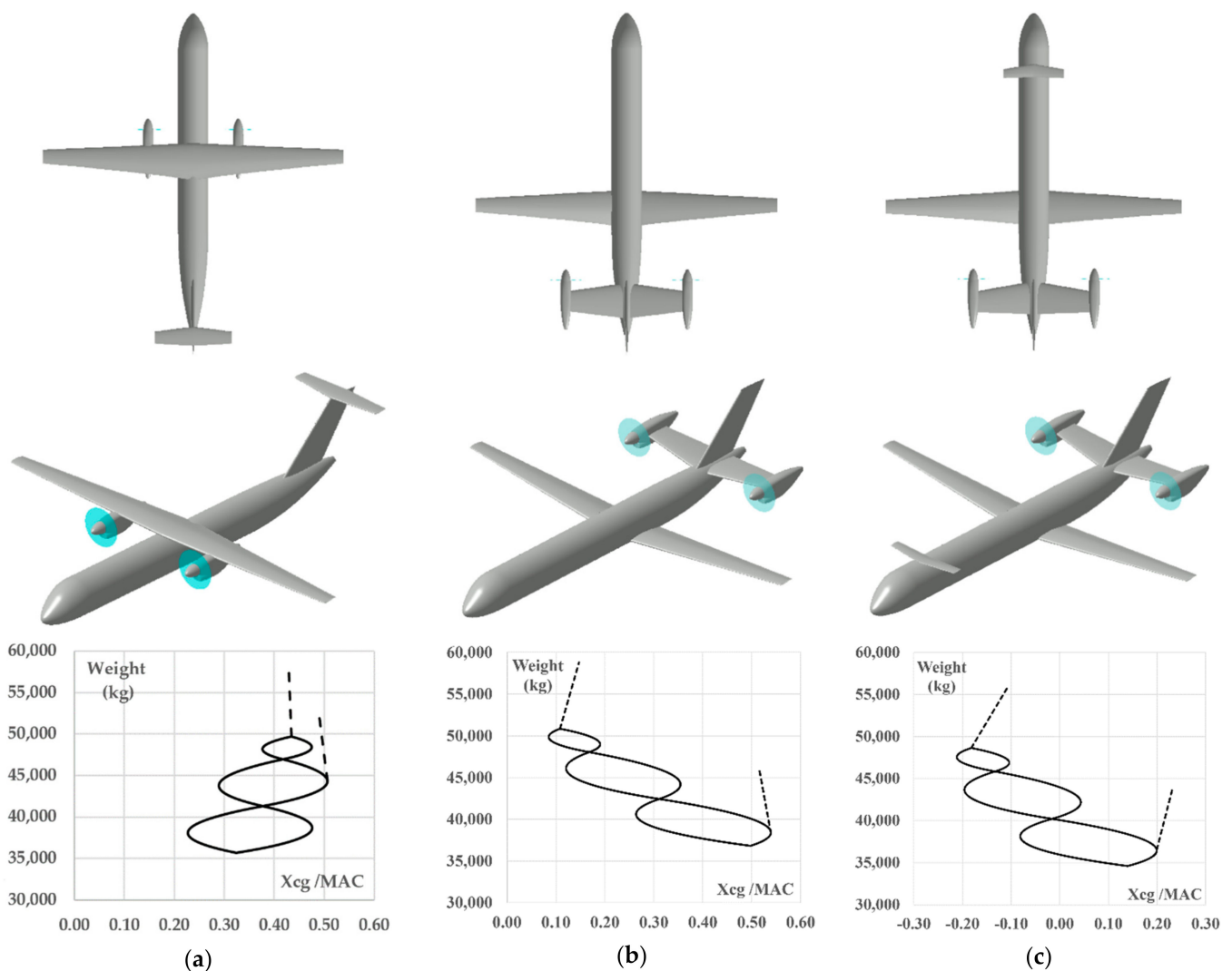


Figure 13. Selected optima solutions for each aircraft configuration: (a) optimized high wing with under wing-mounted engines configuration and its boarding diagram; (b) optimized low wing with rear-mounted engines configuration and its boarding diagram; and (c) optimized three-lifting-surface with rear-mounted engines configuration and its boarding diagram.

Table 4. Comparison between optima large capacity turboprop configurations.

Parameters	Wing Mounted Engines	Rear Mounted Engines	Three-Lifting-Surface
Wing area, S_W (m ²)	104.4	104.6	101.2
Horizontal tail area, S_H (m ²)	16.83	46.5	44.82
Vertical tail area, S_V (m ²)	25.0	25.0	25.0
Canard area, S_C (m ²)	-	-	9.37
Wing aspect ratio, AR_W	12.07	12.04	12.02
Horizontal tail aspect ratio, AR_H	5.00	4.40	4.40
Vertical tail aspect ratio, AR_V	1.37	1.37	1.37
Canard aspect ratio, AR_C	-	-	5.57
Fuselage length, l_f (m)	38.04	38.04	38.04
Fuselage diameter, d_f (m)	3.535	3.535	3.535
Single engine static thrust, T_0 (lbf)	23,603	26,054	23,027
Single Engine Mass (kg)	3367	4122	3297
Max Take-Off Weight (kg)	57,419	58,794	56,640
Operating Empty Weight (kg)	35,665	36,820	34,593
Design Payload (kg)	14,040	14,040	14,040
Max forward CG (% MAC)	22.7%	8.5%	1.2%
Max afterward CG (% MAC)	50.6%	53.9%	23.3%
Aerodynamic cruise efficiency (at 97% MTOW)	16.7	16.6	17.6
Maximum aerodynamic cruise efficiency	18.4	17.8	18.8
Static Stability Margin (%)	3.64	1.16	1.95
C_{Lmax}	1.63	1.57	1.79
$C_{Lmax, TO}$	2.39	2.30	2.52
$C_{Lmax, LND}$	2.97	2.86	3.10
Take-Off Field Length (m)	1396	1380	1380
Landing Field Length (m)	1339	1384	1336
Climb Time (1500 ft–25,000 ft at 190 kt) (min)	15.0	13.0	15.7
Max Cruise Mach Number	0.64	0.67	0.66
Block time—1600 NM (min)	239	234	237
Block fuel—1600 NM (kg)	6259	6479	5958
Total DOC—1600 NM (€ / seat NM)	13.02	12.95	12.83
Cash DOC—1600 NM (€ / seat NM)	7.68	7.70	7.54

By comparing the three-lifting-surface configuration with the rear-mounted engines configuration, the single engine mass is reduced by about 1000 kg (2000 kg for both engines), which justifies the difference in the maximum take-off weight and the lower value of the three-lifting-surface configuration block fuel. On the other hand, the comparison between the three-lifting-surface model and the high wing with wing-mounted engines configuration highlights similar static thrust and engine weight values. However, the reduced aerodynamic efficiency of the wing-mounted engines configuration, due to the set of assumptions shown in Figure 8, coupled with a heavier fuselage led to higher values of both maximum take-off weight and block fuel with respect to the three-lifting-surface model.

A reduced block fuel mass is also linked to a lower amount of pollutant emissions (at fixed engine database); thus, the three-lifting-surface configuration resulted to be the greenest among the investigated configurations. Moreover, thanks to a lighter structure (lowest Operating Empty Weight (OEW)) and the reduced amount of fuel needed for the design mission of 1600 NM, this aircraft also provided the lowest total DOC and cash DOC. Those are mainly influenced by the block fuel mass, the block time, and the aircraft utilization, expressed in terms of block hours per year and calculated as proposed in the book by Kundu [27].

The reference regional jet aircraft was modeled using the JPAD software considering a set of TLARs related to the Airbus A220-300. The main information concerning this aircraft was retrieved from several public sources, including the aircraft manual, the European

Aviation Safety Agency (EASA) type-certificate data sheets, public aircraft data archives, and the Base of Aircraft Data (BADA) database considering aircraft models similar to the A220-300 [28–32]. A data summary of the most important aircraft characteristics is provided in Table 5.

Table 5. Main data concerning the A220-300.

TLAR	
Accommodation (Typical-Full Economy)	135
Design range (typical)	3100 NM
Take-Off Field Length (Max Take-Off Weight, ISA conditions, Sea Level)	1890 m
Landing Field Length (Max Take-Off Weight, ISA conditions, Sea Level)	1509 m
Cruise Mach number (typical)	0.78
Cruise altitude (typical)	37,000 ft
Max cruise Mach number at 37,000 ft	0.82
Max operating altitude	41,000 ft
Alternate cruise range (assumed by authors)	200 NM
Alternate cruise altitude (assumed by authors)	20,000 ft
Holding duration (assumed by authors)	30 min
Holding altitude (assumed by authors)	1500 ft/min
Residual fuel reserve (assumed by authors)	5%
Geometrical and Operational Data	
Wing area	112.3 m ²
Wingspan	35.1 m
Wing aspect ratio	10.97
Fuselage length	38.71 m
Fuselage diameter	3.7 m
Single engine static thrust	24,400 lbf
Engine by-pass ratio	12:1
Max Take-Off Weight	67,585 kg
Max Landing Weight	58,740 kg
Max Zero-Fuel Weight	55,792 kg
Operating Empty Weight	37,081 kg
Max Payload	18,711 kg
Max Fuel Mass	17,726 kg
BADA averaged climb speed (CAS)	271 kt
BADA averaged rate of climb	1642 ft/min
BADA maximum rate of climb	2862 ft/min
BADA averaged descent speed (CAS)	218 kt
BADA averaged rate of descent	2186 ft/min
BADA maximum rate of descent	3700 ft/min

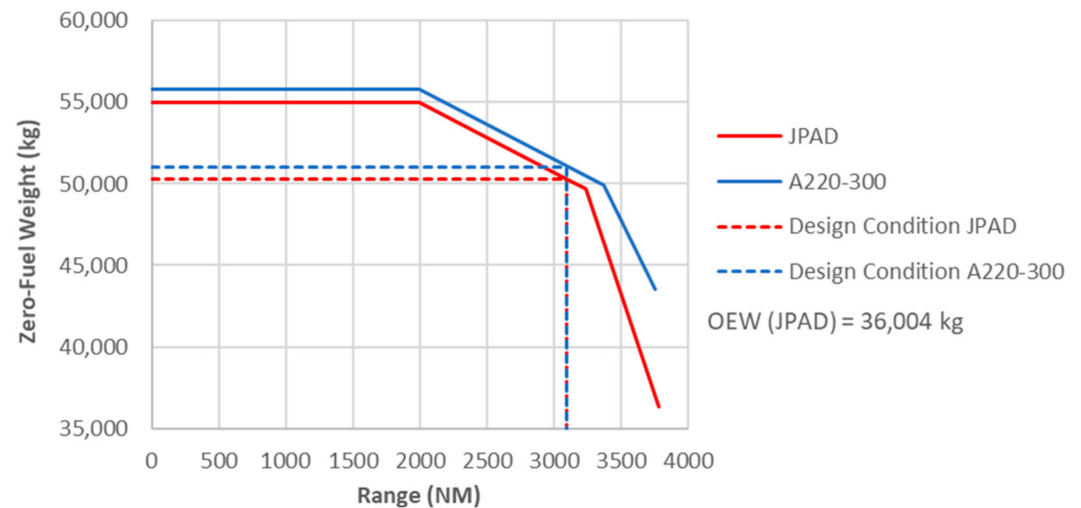
A complete case study concerning this aircraft model and its implementation inside the JPAD software was carried out by authors and reported in [33]. Here, starting from publicly available data concerning the aircraft geometry and using the aircraft 3-views for the geometry digitization process, a parametric model was generated. The latter was used to perform a complete multi-disciplinary analysis cycle, as described in Figure 6, neglecting the static thrust update loop but including the mission fuel feedback loop.

It must be noted that, in terms of DOC, the fuel price value needed to perform the analysis was assumed according to IATA fuel price monitor [34], while aircraft price was assumed considering reference data reported in [35]. Engine unit costs were deducted from [36] as well.

The main output of the JPAD multi-disciplinary analysis was compared with aircraft data reported in Table 5 to validate the calculation case. A summary of this comparison is reported in Table 6, while a comparison in terms of payload–range diagram is provided in Figure 14, where the main differences between the two charts can be addressed to the gap between the values of the Max Zero-Fuel Weight (MZFW), the OEW, and the max fuel mass of the A220-300 with respect to the values calculated by JPAD.

Table 6. Comparison between JPAD output and A220-330 data in Table 5.

Parameters	JPAD	A220-300 (Table 5)	Difference (%)
Max Take-Off weight (kg)	66,911	67,585	−1.00%
Max Landing weight (kg)	56,875	58,740	−3.18%
Max fuel mass (kg)	17,233	17,726	−2.78%
Max Zero-Fuel Weight (kg)	55,017	55,792	−1.39%
Operating Empty Weight (kg)	36,306	37,081	−2.09%
Take-Off Field Length (m)	1814	1890	−4.02%
Landing Field Length (m)	1575	1509	+4.37%

**Figure 14.** Payload–range chart calculated with JPAD compared with the A220-300 Payload-Range chart. Adapted from ref. [28].

Once the A220-300 JPAD model was validated, it was used to perform an additional simulation considering the design range from the set of TLARs in Table 1. In addition, to compare this reference regional jet with all three optimal turboprop aircraft layouts, its payload mass was modified to comply with the design payload of 14,040 kg used for each high-capacity turboprop configuration.

Finally, a comparison between the three optimal configurations and a reference regional jet platform, assumed as the Airbus A220-300, is presented in Table 7 considering a mission of 1600 NM.

As shown in Table 7, all high-capacity turboprop configurations provide a beneficial effect on the amount of block fuel related to the design mission of 1600 NM. However, it must be noted that the considered reference regional jet is designed for a mission range of 3300 NM, thus the aerodynamic efficiency and the take-off weight are not optimized for a 1600 NM mission range. Although this seems to be an unfair comparison, it must be highlighted that this study aims to compare the benefit in terms of fuel consumption that a new large capacity turboprop, specifically designed for short/medium haul, would have with respect to the existing state-of-the-art RJ also currently operated on this kind of missions.

In addition to this comparison, the authors also designed a possible new regional jet aircraft using the same set of TLARs of the turboprop aircraft. Only the cruise Mach number was shifted from 0.64 to 0.78 since this is a jet-driven aircraft. This comparison, shown in Table 7, was added to demonstrate that, even if a regional jet specifically designed on such a mission range existed, the proposed large turboprop aircraft would still provide benefits in terms of environmental impact. The major drawback of the turboprop solution is represented by a higher total DOC value mainly due to the reduced block speed.

Table 7. Comparison with the reference regional jet in terms of block time, block fuel, and DOC (percent differences, in brackets, with respect to the regional jet).

Design Mission: 1600 NM	Wing Mounted Engines	Rear Mounted Engines	Three-Lifting- Surface	RJ Designed at 1600 NM	Ref. RJ
Take-off weight (kg)	57,419 (−3.11%)	58,794 (−0.79%)	56,640 (−4.42%)	54,378 (−8.24%)	59,260
Cruise Mach number	0.64 (−17.95%)	0.67 (−14.10%)	0.66 (−15.38%)	0.78 (+0.0%)	0.78
Aerodynamic Cruise efficiency	16.7 (0.0%)	16.6 (−0.60%)	17.6 (+5.38%)	17.2 (+2.99%)	16.7
Relative cruise SFC (w.r.t. RJ)	−19.22%	−17.02%	−18.56%	−	−
Utilization (h/year)	3353 (+0.60%)	3346 (+0.39%)	3350 (+0.51%)	3329 (−0.12%)	3333
Block Time (min)	239 (+6.22%)	234 (+4.00%)	237 (+5.33%)	222 (−1.33%)	225
Block Fuel (kg)	6259 (−10.40%)	6479 (−7.24%)	5958 (−17.24%)	6569 (−5.96%)	6985
Total DOC (¢/seat*NM)	13.02 (−13.37%)	12.95 (−13.84%)	12.83 (−14.63%)	12.03 (−19.96%)	15.03
Cash DOC (¢/seat*NM)	7.68 (−7.69%)	7.70 (−7.45%)	7.54 (−9.37%)	8.32 (+0.00%)	8.32

The design of this new regional jet was accomplished using the same multi-disciplinary analysis and optimization workflow adopted for all proposed turboprop configurations. Starting from the TLARs shown in Table 1 and considering as baseline the JPAD parametric model of the A220-300, the set and ranges of design parameters reported in Table 8 were considered.

Table 8. Variables design space for the regional jet model designed on a 1600 NM mission profile.

Parameters	Wing Design Parameters
Span b_w (m)	32.0–35.1
Longitudinal position $X_{LE,W}$ (m)	10.0–13.0
Aspect Ratio AR_w	9.10–12.19
Sweep at leading edge $\Lambda_{LE,W}$ (°)	25.0–35.0
Horizontal Tailplane Design Parameters	
Span b_H (m)	10.75–13.14
Longitudinal position $X_{LE,H}$ (m)	31.6 fixed value
Aspect Ratio AR_H	5.12 fixed value
Sweep at leading edge $\Lambda_{LE,H}$ (°)	$\Lambda_{LE,W} + 5.0$

The optimization problem carried out for this aircraft is represented in Equation (2) where the block fuel was assumed as the only objective function. It must be noted that the optimization problem is the same as the one considered for all turboprop aircraft, except for the time to climb condition and the cruise Mach number, which was considered to change in the range from 0.78 to 0.82 corresponding to the typical and maximum Mach numbers of the A220-300, respectively. The previous climb time condition was not included in the set of constraints since this aircraft is supposed to operate at a higher cruise altitude (37,000 ft instead of 30,000 ft).

$$\left\{ \begin{array}{l}
 \text{Minimize the Block fuel on a mission range of 1600 NM} \\
 \text{with respect to lifting surfaces planform design variables and relative positioning} \\
 \text{subject to :} \\
 \text{S.S.M} \geq 0.0 \\
 \text{Take – off field length \& Landing field length} \leq 1400 \text{ m} \\
 \text{Cruise Mach number } 0.78 \leq M_{cr} \leq 0.82 \\
 \|X_{LG} - X_{CG,max,alt}\| \geq 5\%MAC \\
 \text{Estimated mission fuel} \leq \text{Max storable fuel mass}
 \end{array} \right. \quad (2)$$

The MDA workflow adopted for the analysis of each regional jet models included in the design space was the same as the one shown in Figure 6, where the engine static thrusts were modified iteratively to match the requirements in terms of cruise Mach number and take-off field length. However, the rubberized engine database used for the performance

simulation was the same used to analyze the A220-300 parametric model, thus the same SFC was considered at fixed altitude and cruise Mach number.

To make a fair comparison with the optima turboprop solutions, the selection of the optimum regional jet aircraft was driven by the minimization of the block fuel targeting the lowest environmental impact. The DOC was estimated only for comparison purposes.

A geometrical comparison between the baseline regional jet model and the selected optimum jet aircraft is shown in Figure 15.

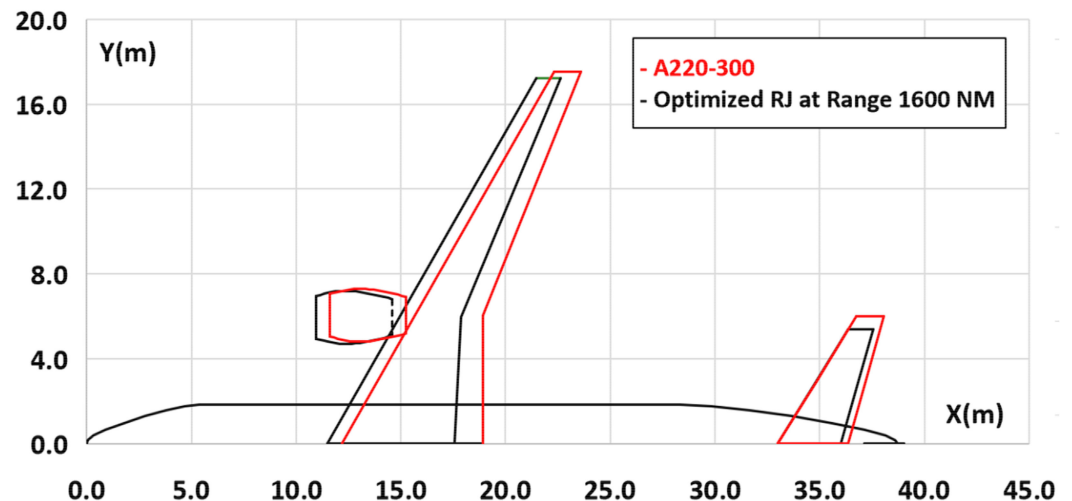


Figure 15. Comparison between top views of the baseline regional jet model (red) and the selected optimum regional jet aircraft (black).

Starting from the results shown in Table 7, a first comparison that can be made is between the proposed turboprop solutions and the existing state of the art regional jet (the last column of Table 7) typically operated on short/medium haul with a seats capacity similar to the required value of 130.

Focusing on each turboprop platform, the high-wing configuration with wing-mounted engines has the greatest advantage in terms of mean cruise SFC with a reduction of -19.22% and provides for the second best reduction in take-off weight (-3.11%). However, the cruise aerodynamic efficiency shows no improvements, with respect to the reference regional jet, and the cruise Mach number is the lowest among all analyzed turboprop aircraft models. Thus, this configuration is the worst in terms of block time providing for an additional little negative effect on the block fuel.

From the combination of all these effects, this aircraft may be a good candidate to challenge a regional jet on this kind of missions with an overall block fuel reduction of 0.40% and only 15 min of additional block time. In term of DOC, good results were reached as well, with a reduction of -13.37% in total DOC and -7.68% in cash DOC. However, despite the beneficial effect provided by the smaller block fuel mass, this aircraft is the worst in terms of both utilization and block time, leading to the lowest reduction in total DOC. On the other hand, being the effect of the block fuel much more effective on the cash DOC rather than on the total DOC, this configuration provides for a slightly lower cash DOC value with respect to the one with low-wing and rear-engine installation.

The second high-capacity turboprop configuration showed the lowest reduction in term of block fuel (-7.24%), with respect to the reference regional jet, since the beneficial effect provided by the smaller value of the mean cruise SFC (-17.02%) is mitigated by a very little reduction in MTOW (-0.79%) and a lower value of the cruise aerodynamic efficiency (-0.60%). On the other hand, the cruise Mach number was the greatest among all analyzed turboprop configurations, leading to the lowest increment in block time with respect to the reference regional jet. However, being this effect very limited, the related effect on the block fuel is also very limited. In terms of DOC, comparing this configuration with all other turboprop platforms, the lower block time provides for a better value of the

utilization parameter which positively affects all costs contributions. Major drawbacks are provided by the increased amount of block fuel (and so of the fuel price) and by the take-off weight (the highest among all turboprop configurations) which influences maintenance costs. However, those effects are smaller than the one provided by the utilization, making this aircraft the second best solution in terms of total DOC reduction with respect to the reference regional jet. As for the previous case, the effect of the block fuel on the cash DOC is much more effective than on the total DOC, providing for the worst reduction of this value.

As stated above, the three-lifting-surface configuration resulted to be the best turboprop configuration. This was further confirmed by the comparison with the reference regional jet, from which this innovative high-capacity turboprop aircraft has highlighted the greatest reduction both in term of block fuel and DOC. In particular, this aircraft provided a mean cruise SFC reduction similar to the first configuration (-18.56% instead of -19.22%) together with the lowest value of the take-off weight and the highest value of the cruise aerodynamic efficiency (-4.42% and $+5.38\%$, respectively, if compared to the reference regional jet). A cruise Mach number slightly lower than the second configuration led to intermediate values of both block time and utilization between the first two analyzed aircraft models.

A second comparison that can be made is between the proposed turboprop solutions with the regional turboprop designed according to the same set of TLARs.

Considering that this aircraft was optimized on the same set of TLARs adopted for each turboprop aircraft, the amount of block fuel needed to operate the 1600 NM design mission is obviously reduced with respect to the one related to the A220-300 parametric model. Although with block fuel values in line with some of the analyzed optima turboprop models, the three-lifting-surface configuration still provide for a beneficial effect in terms of environmental impact with respect to this possible regional jet model achieving a fuel saving of about 611 kg (-9.30%).

Conversely, the new regional jet represents the best solution in terms of total DOC having both an improved block time with respect to the optima turboprop aircraft and the lowest take-off weight. In particular, by comparing the three-lifting-surface configuration with this newly designed regional jet, there is a total DOC increment of about $+6.65\%$. However, dealing with the cash DOC, which is not influenced by the beneficial effect provided by a reduced take-off weight, the three-lifting-surface configuration allows achieving the same cost saving shown with respect to the A220-300 model of about -9.37% . Thus, the proposed three-lifting-surface configuration represents the best solution in terms of both environmental impact and cash DOC.

5. Conclusions

This paper considers the possible design of a modern high-capacity turboprop aircraft that could potentially reduce the environmental impact of regional aircraft with respect to the current state-of-the-art regional jet widely adopted on short/medium hauls. The study investigated three possible architectural solutions for a large capacity turboprop aircraft. A multi-disciplinary analysis and optimization process was carried out to assess the best solution complying with the imposed design space boundaries and operative constraints.

By comparing the results obtained for each optimum turboprop aircraft with respect to a reference regional jet model, represented by the Airbus A220-300 operated on a range of 1600 NM, this study highlighted a maximum potential fuel saving of about -17.24% considering a three-lifting-surface configuration.

In addition, to make a fair comparison between the analyzed turboprop aircraft platforms and a regional jet, a brand-new turbofan aircraft was designed using the same set of TLARs used for the turboprop configurations. It must be noted that such a regional jet aircraft, coupling a design range of 1600 NM with a seat capacity of 130 passengers, does not exist in the current regional market scenario. By comparing the best analyzed turboprop configuration with this regional jet model, the initial block fuel saving of 7.24% reaches a

lower value of -5.96% , still proving that a modern optimized turboprop platform could provide for a beneficial effect in terms of environmental impact.

For the sake of completeness, a comparison between all optimal turboprop configurations and both the analyzed regional jet models was carried out also in terms of DOC. Starting with the existing reference regional jet model, being the latter not optimized on a 1600 NM mission range, all turboprop models provide for a cost reduction in terms of both total and cash DOC (max reduction of about -14.63%). However, considering a regional jet specifically designed for such a mission range, it can be highlighted that the jet aircraft represents the best solution in terms of total DOC (-6.65% with respect to the best analyzed turboprop configuration) but not in terms of cash DOC due to the higher block fuel ($+9.37\%$ with respect to the best analyzed turboprop configuration).

Since this work is not focused on the investigation of the best possible turboprop aircraft architecture, implementing future technologies or layouts, the performed investigation only considered three possible configurations of a large capacity turboprop assumed to be compliant with an entry into service by the year 2035. A wider study, extended to a larger portfolio of innovative, or even disruptive, configurations should be performed to find a better solution with respect to the one proposed in this paper.

Author Contributions: Conceptualization, S.C.; funding acquisition, F.N.; investigation, S.C. and V.T.; methodology, S.C. and V.T.; software, S.C., V.T. and A.D.M.; supervision, F.N.; writing—original draft, S.C. and V.T.; writing—review & editing, F.N. and A.D.M. All authors have read and agreed to the published version of the manuscript.

Funding: The presented research activities represents part of a wider investigation that was performed and funded for the discussed innovative regional turboprop platform by the IRON project. The IRON project has received funding from the Clean Sky 2 Joint Undertaking under the European Union's Horizon 2020 research and innovation program under Grant Agreement No. 699715. The IRON project is part of Clean Sky 2 REG-GAM 2018 project implemented on the H2020 program under GA 807089.

Institutional Review Board Statement: Not applicable.

Informed Consent Statement: Not applicable.

Data Availability Statement: The data presented in this study are available on request from the corresponding author. Since this work has its roots in findings of a European research project involving several industrial partners data are not publicly available.

Conflicts of Interest: The authors declare no conflict of interest.

Abbreviations

The following abbreviations are used in this manuscript.

APU	Auxiliary Power Unit
ATAG	Air Transport Action Group (www.atag.org)
ATR	Avions de Transport Régional (www.atr-aircraft.com)
BADA	Base of Aircraft Data (www.eurocontrol.int/model/bada)
CAS	Calibrated Air Speed
CG	Center of Gravity
CS2	Clean Sky 2 (www.cleansky.eu)
DOC	Direct Operating Cost
DOE	Design of Experiments
EASA	European Aviation Safety Agency (www.easa.europa.eu)
EU	European Union
FAA	United States Federal Aviation Administration (www.faa.gov)
FL	Flight Level

IATA	International Air Transport Association (www.iata.org)
ICAO	International Civil Aviation Organization (www.icao.int/Pages/default.aspx9)
IRON	Innovative turbopROp configuration
ISA	International Standard Atmosphere
JPAD	Java tool chain of Programs for Aircraft Design
LFL	Landing Field Length
LG	Landing Gear
MAC	Mean Aerodynamic Chord
MDA	Multi-Disciplinary Analysis
MDAO	Multi-Disciplinary Analysis and Optimization
MLW	Maximum Landing Weight
MTOW	Maximum Take-Off Weight
MZFW	Max Zero-Fuel Weight
NASA	United States National Aeronautics and Space Administration (www.nasa.gov)
NLF	Natural Laminar Flow
OEW	Operating Empty Weight
RJ	Regional Jet
S.S.M.	Static Stability Margin
SFC	Specific Fuel Consumption
TLARs	Top-Level Aircraft Requirements
TOFL	Take-Off Field Length

Symbols

The following symbols are used in this manuscript.

¢	United States dollar cent
AR_C	canard aspect ratio
AR_H	horizontal tailplane aspect ratio
AR_V	vertical tail aspect ratio
AR_W	wing aspect ratio
b_C	canard span
b_H	horizontal tailplane span
b_W	wingspan
$C_{L\alpha,H}$	horizontal tail lift curve slope
C_{Lmax}	maximum lift coefficient
$C_{Lmax,LND}$	maximum lift coefficient at landing
$C_{Lmax,TO}$	maximum lift coefficient at take-off
C_{O_2}	carbon dioxide
dcS	drag counts
d_f	fuselage diameter
i_H	horizontal tailplane root incidence angle
l_f	fuselage length
M	Mach number
M_{cr}	cruise Mach number
NM	nautical mile
NO_x	nitrogen dioxide
S_C	canard area
S_H	horizontal tailplane area
S_V	vertical tailplane area
S_W	wing area
T_0	single engine static thrust
US\$	United States dollar
$\Lambda_{LE,C}$	canard sweep angle at the leading edge
$\Lambda_{LE,H}$	horizontal tailplane sweep angle at the leading edge
$\Lambda_{LE,W}$	wing sweep angle at the leading edge
X_{cg}	center of gravity longitudinal position
$X_{CG,max,aft}$	max aft center of gravity longitudinal position
$X_{LE,C}$	canard root leading edge longitudinal position
$X_{LE,H}$	horizontal tail root leading edge longitudinal position
$X_{LE,W}$	wing root leading edge longitudinal position
X_{LG}	main landing gear longitudinal position

References

1. Climate Change. Available online: <https://perma.cc/X2GW-2J8N> (accessed on 25 January 2021).
2. Scholz, D. Review of CO₂ Reduction Promises and Visions for 2020 in Aviation. In Proceedings of the Deutscher Luft- und Raumfahrtkongress 2020 (DLRK 2020), Online, 1–3 September 2020. [CrossRef]
3. European Union. Clean Sky 2 Joint Undertaking Development Plan. Available online: <https://perma.cc/JL26-EGYQ> (accessed on 30 April 2021).
4. ICAO, Air Transport Bureau. Effects of Novel Coronavirus (Covid-19) on Civil Aviation: Economic Impact Analysis. Available online: <https://perma.cc/AU9L-48B7> (accessed on 30 April 2021).
5. Airbus. Global Market Forecast 2018–2037. Available online: <https://perma.cc/5WT8-GSDB> (accessed on 30 April 2021).
6. ATR. Turboprop Market Forecast 2018–2037. Available online: <https://perma.cc/X4VZ-JKW8> (accessed on 30 April 2021).
7. Nicolosi, F.; Corcione, S.; Della Vecchia, P.; Trifari, V.; Ruocco, M. Aerodynamic design and analysis of an innovative regional turboprop configuration. In Proceedings of the 31st ICAS Conference (International Council of the Aeronautical Sciences), Belo Horizonte, Brazil, 9–14 September 2018; Available online: <https://hdl.handle.net/11588/736423> (accessed on 30 April 2021).
8. Nicolosi, F.; Corcione, S.; Della Vecchia, P.; Trifari, V.; Ruocco, M.; De Marco, A. Design and aerodynamic analysis of a regional turboprop innovative configuration. In Proceedings of the Aerospace Europe 6th CEAS Conference, Bucharest, Romania, 16–20 October 2017; Council of European Aerospace Societies: Brussels, Belgium, 2017. Available online: <https://hdl.handle.net/11588/696609> (accessed on 30 April 2021).
9. Corcione, S.; Nicolosi, F.; Della Vecchia, P.; Ciliberti, D.; Cusati, V. High lift aerodynamic characteristics of a three lifting surfaces turboprop aircraft. In Proceedings of the AIAA Aviation 2019 Forum, Dallas, TX, USA, 17–21 June 2019; American Institute of Aeronautics and Astronautics: Reston, VA, USA, 14 June 2019. AIAA 2019–2884. [CrossRef]
10. Nicolosi, F.; Corcione, S.; Trifari, V.; Cusati, V.; Ruocco, M.; Della Vecchia, P. Performance evaluation and DOC estimation of an innovative turboprop configuration. In Proceedings of the 2018 Aviation Technology, Integration, and Operations Conference, Atlanta, Georgia, 25–29 June 2018; American Institute of Aeronautics and Astronautics: Reston, VA, USA, 24 June 2018. AIAA 2018–3662. [CrossRef]
11. Nicolosi, F.; Corcione, S.; Ciliberti, D.; Cusati, V. Aerodynamic characteristics of an innovative large turboprop through wind tunnel tests including propulsive effects. In Proceedings of the AIAA AVIATION 2020 FORUM, Virtual Event, 15–19 June 2020; American Institute of Aeronautics and Astronautics: Reston, VA, USA, 8 June 2020. AIAA 2020–2623. [CrossRef]
12. Cusati, V.; Nicolosi, F.; Corcione, S.; Ciliberti, D.; Della Vecchia, P. Longitudinal stability issues including propulsive effects on an innovative commercial propeller-driven aircraft. In Proceedings of the AIAA Aviation 2019 Forum, Dallas, TX, USA, 17–21 June 2019; American Institute of Aeronautics and Astronautics: Reston, VA, USA, 14 June 2019. AIAA 2019–2882. [CrossRef]
13. Bombardier Commercial Aircraft. Market Forecast 2017–2036. Available online: <https://perma.cc/9Q7A-753T> (accessed on 30 April 2021).
14. Goldsmith, M. *A Study to Define the Research and Technology Requirements for Advanced Turbo/Propfan Transport Aircraft*; NASA: Washington, DC, USA, 1981. Available online: <https://core.ac.uk/display/42857722> (accessed on 30 April 2021).
15. Whitlow, J.B., Jr.; Siviers, G.K. *Fuel Savings Potential of the NASA Advanced Turboprop Program*; NASA: Washington, DC, USA, 1984. Available online: <https://core.ac.uk/display/42848326> (accessed on 30 April 2021).
16. Sullivan, W.E.; Turnberg, J.E.; Violette, J.A. *Large-Scale Advanced Prop-Fan (Lap) Blade Design*; NASA: Washington, DC, USA, 1984. Available online: <https://core.ac.uk/display/42834130> (accessed on 30 April 2021).
17. Johanning, A.; Scholz, D. Novel Low-Flying Propeller-Driven Aircraft Concept for Reduced Direct Operating Costs and Emissions. In Proceedings of the 28th Congress of the International Council of the Aeronautical Sciences, ICAS 2012, Brisbane, Australia, 23–28 September 2012; Optimage Ltd.: Edinburgh, UK, 2012. ISBN 978-0-9565333-1-9. Available online: <http://Airport2030.ProfScholz.de> (accessed on 30 April 2021).
18. Johanning, A.; Scholz, D. Investigation of a Novel Turboprop-Driven Aircraft Concept Including Future Technologies. In *Innovative Design and Development Practices in Aerospace and Automotive Engineering*; Bajpai, R., Chandrasekhar, U., Eds.; Springer: Singapore, 2016; Lecture Notes in Mechanical Engineering; Available online: <http://india.ProfScholz.de> (accessed on 28 April 2021). [CrossRef]
19. Vos, R.; Hoogreef, M.F.M. A System-Level Assessment of Tail-Mounted Propellers for Regional Aircraft. In Proceedings of the 31st ICAS Conference (International Council of the Aeronautical Sciences), Belo Horizonte, Brazil, 9–14 September 2018; Available online: <http://resolver.tudelft.nl/uuid:a1674c88-2df1-4365-8c3a-efde47de7f8c> (accessed on 30 April 2021).
20. ICAO Aerodrome Reference Code. Available online: <https://perma.cc/UD6U-EUJ9> (accessed on 30 April 2021).
21. Nicolosi, F.; De Marco, A.; Attanasio, L.; Della Vecchia, P. Development of a java-based framework for aircraft preliminary design and optimization. *J. Aerosp. Inf. Syst.* **2016**, *13*, 234–242. [CrossRef]
22. De Marco, A.; Cusati, V.; Trifari, V.; Ruocco, M.; Nicolosi, F.; Della Vecchia, P. A Java Toolchain of Programs for Aircraft Design. In Proceedings of the Aerospace Europe 6th CEAS Conference, Bucharest, Romania, 16–20 October 2017; Council of European Aerospace Societies: Brussels, Belgium, 2017. Available online: <http://hdl.handle.net/11588/696606> (accessed on 30 April 2021).
23. Trifari, V.; Ruocco, M.; Cusati, V.; Nicolosi, F.; De Marco, A. Multi-Disciplinary Analysis and Optimization Java Tool for Aircraft Design. In Proceedings of the 31st ICAS Conference (International Council of the Aeronautical Sciences), Belo Horizonte, Brazil, 9–14 September 2018. Available online: <http://hdl.handle.net/11588/748237> (accessed on 30 April 2021).

24. De Marco, A.; Trifari, V.; Nicolosi, F.; Ruocco, M. A Simulation-Based Performance Analysis Tool for Aircraft Design Workflows. *Aerospace* **2020**, *7*, 155. [[CrossRef](#)]
25. Torenbeek, E. *Synthesis of Subsonic Airplane Design*; Delft University Press: Delft, The Netherlands, 1976; ISBN 978-94-017-3202-4. Available online: <http://resolver.tudelft.nl/uuid:229f2817-9be9-49b6-959a-d653b5bac054> (accessed on 30 April 2021).
26. Schouten, T.J.E. Assessment of Conceptual High-Capacity Regional Turbopropeller Aircraft. Master's Thesis, Aerospace Engineering at Delft University of Technology, Delft, The Netherlands, 30 April 2018. Available online: <http://resolver.tudelft.nl/uuid:236ad212-eb0b-443d-a40d-602ec6fe64f9> (accessed on 30 April 2021).
27. Kundu, A.K. *Aircraft Design*; Cambridge University Press: Cambridge, UK, 2010; ISBN 9780511844652. [[CrossRef](#)]
28. Airport Planning Publication. Tech. Rep. BD500-3AB48-32000-00 Issue 13. Available online: <https://perma.cc/PKT3-K4QP> (accessed on 30 April 2021).
29. Type-Certificate Data Sheet for BD-500 (A220 Series). In *Tech. Rep. EASA.IM.A.570*; European Aviation Safety Agency (EASA): Cologne, Germany, 2019. Available online: <https://perma.cc/2TUL-KALL> (accessed on 30 April 2021).
30. Type-Certificate Data Sheet for PW1500G Series Engines. In *Tech. Rep. EASA.IM.A.090*; European Aviation Safety Agency (EASA): Cologne, Germany, 2018. Available online: <https://perma.cc/L243-JHZU> (accessed on 30 April 2021).
31. BOMBARDIER BD-500 C Series CS300. Available online: <https://perma.cc/J26A-U69U> (accessed on 30 April 2021).
32. Nuic, A.; Poles, D.; Mouillet, V. BADA: An advanced aircraft performance model for present and future ATM systems. *Int. J. Adapt. Control Signal Process.* **2010**, *24*, 850–866. [[CrossRef](#)]
33. Trifari, V. Development of a Multi-Disciplinary Analysis and Optimization Framework and Applications for Innovative Efficient Regional Aircraft. Ph.D. Thesis, University of Naples Federico II, Naples, Italy, 17 April 2020.
34. Jet Fuel Price Monitor. Available online: <https://perma.cc/S3KC-WNV4> (accessed on 30 April 2021).
35. Airbus 2018 Price List Press Release. Available online: <https://perma.cc/42VR-39YS> (accessed on 30 April 2021).
36. JetBlue Picks Pratt over CFM for Engines Valued at \$1.03 Billion. Available online: <https://perma.cc/AL3M-Z8EJ> (accessed on 30 April 2021).